Nanoscale Res Lett (2010) 5:1822–1828
DOI 10.1007/s11671-010-9719-6

NANO EXPRESS

Synthesis and Photoluminescence Properties of Porous Silicon Nanowire Arrays

Linhan Lin · Siping Guo · Xianzhong Sun · Jiayou Feng · Yan Wang

Received: 27 May 2010 / Accepted: 26 July 2010 / Published online: 5 August 2010

Abstract Herein, we prepare vertical and single crystalline porous silicon nanowires (SiNWs) via a two-step metal-assisted electroless etching method. The porosity of the nanowires is restricted by etchant concentration, etching time and doping lever of the silicon wafer. The diffusion of silver ions could lead to the nucleation of silver nanoparticles on the nanowires and open new etching ways. Like porous silicon (PS), these porous nanowires also show excellent photoluminescence (PL) properties. The PL intensity increases with porosity, with an enhancement of about 100 times observed in our condition experiments. A "red-shift" of the PL peak is also found. Further studies prove that the PL spectrum should be decomposed into two elementary PL bands. The peak at 850 nm is the emission of the localized excitation in the nanoporous structure, while the 750-nm peak should be attributed to the surface-oxidized nanostructure. It could be confirmed from the Fourier transform infrared spectroscopy analyses. These porous SiNW arrays may be useful as the nanoscale optoelectronic devices.

Keywords Porous silicon nanowires · Electroless etching · Silver catalyst · Photoluminescence · Porosity

L. Lin · S. Guo · X. Sun · J. Feng (✉)
Department of Materials Science and Engineering, Key Lab of Advanced Materials, Tsinghua University, 100084 Beijing, People's Republic of China
e-mail: fengjy@mail.tsinghua.edu.cn

Y. Wang
Institute of Microelectronics of Tsinghua University, 100084 Beijing, People's Republic of China

Introduction

Silicon with nanoscale has received much attention due to its potential applications on electronics, photonics, nanoscale sensors and renewable energy. Several silicon nanostructures, such as porous silicon (PS), silicon nanowires (SiNWs) and silicon nanocrystals, were proposed over the past decade. Due to their unique one-dimensional physical properties, SiNWs were explored for field effect transistors [1–4], chemical or biological sensors [5–9], battery electrodes [10, 11] and photovoltaics [12–14]. However, the application of silicon is still greatly restricted due to its indirect energy band gap, especially in the field of optically active material and optoelectronics. Silicon nanocrystals [15, 16] and PS [17, 18] are thought to be possible candidate systems in solving this physical inability and act as effective light emitters. PS is typically prepared by applying a voltage bias to a silicon substrate immersed in the ethanol and hydrofluoric acid mixture. The metal-assisted chemical etching process was also used to prepare PS [19] and SiNWs [20–24] as well. Few attempts were focused on the luminescence of SiNWs [25–29]. Recently, it is found that this method can be used to synthesize a new silicon nanostructure named Porous SiNWs [30, 31], which could combine the physical feature of SiNWs and PS. It is also possible to gain a large area uniform array controllable and repeatable. It is expected this could open a new opportunity for the silicon based optoelectronics and photoelectrochemical devices.

In this work, we synthesized porous SiNWs with different parameters, including the etchant concentration, etching time and post-treatment. The variable morphology of the SiNWs is present, and the etching mechanism is discussed. The photoluminescence (PL) properties dependent on the processing parameters are also investigated here.

Experiment Details

SiNW arrays were prepared by Ag-assisted chemical etching of *n*-Si (100) wafers with the resistivity of about 0.02 Ω cm. The samples were firstly washed with acetone and deionized water and then immersed into H_2SO_4 and H_2O_2 solution in a volume ration of 3:1 to remove the organic contaminants on the surface. The thin oxide layer formed on the surface was then dissolved in a 5% HF solution. This treated wafer was transferred into an Ag deposition solution containing 4.8 M HF and 0.005 M $AgNO_3$ for 1 min at room temperature. The Ag nanoparticles (AgNPs) coated samples were sufficiently rinsed with deionized water to remove extra silver ions and then soaked into an etchant bath. The HF concentration of the etching solutions is 4.8 M, while the H_2O_2 concentrations vary from 0.1 to 0.5 M. The etching times are 30, 60, 90, 120 and 180 min, respectively. The Ag metal was dissolved with nitric acid. Then, each sample was divided into two parts, one of which was immersed into 5% HF solution to remove the oxide layer induced by the nitric acid. Finally, the wafers were cleaned with water and dried under N_2 flow.

The SiNW arrays were characterized by scanning electron microscopy (SEM) using JEOL JSM-6460LV, Thermally-Assisted Field Emission SEM (LEO 1530) and TEM (JEOL-200CX). The local atomic environments and bonding configurations in the samples were examined by Fourier transform infrared spectroscopy (FTIR) using Nicolet 6700. The PL measurements were conducted using an *X Y* triple spectrograph equipped with a liquid N_2-cooled CCD camera. A 514.5-nm line Ar^+ laser was employed to excite the luminescence with a spot size of about 5 μm in diameter and excitation power of 0.1 mW. All PL spectra were taken at room temperature.

Results and Discussion

SEM and TEM images of the as-grown SiNWs etched with different H_2O_2 concentrations for 1 h are summarized in Fig. 1. The nanowires distribute uniformly on the whole wafers and are vertical to the substrate surface. The nanowires etched with lower H_2O_2 concentrations are isolated from each other. However, when the concentration of H_2O_2 increases, the tips of the nanowires congregate together. The diameters of the congregated bundles are several micrometers from the top view. These congregated bundles are also uniformly distributed on the entire wafers and could be confirmed from the cross-section images. From the TEM images, it is found that the surface of the nanowires becomes rough and the porosity (or the density) of the nanopores increases with H_2O_2 concentration. From our condition experiments, we found that the nanopores appear from the lowest H_2O_2 concentration of 0.1 M, for which the pores are smaller (several nanometers) and porosity is rather low. This is different from the earlier report [31] which pointed out that the nanopores did not appear, but only rough surface was found until the H_2O_2 concentration was high enough. With the increase of H_2O_2 concentrations, the pores also seem to grow, with the diameters ranging from several nanometers to nearly 10 nm for higher H_2O_2 concentrations. The diffraction pattern in Fig. 1o indicates the nanowire is single crystalline. We also prepared SiNWs with the same H_2O_2 concentration of 0.3 M, but different etching times from 30 min to 3 h. The morphology of these SiNWs is summarized in Fig. 2. The variable morphology of the SiNWs with etching time is similar to the concentration of the etchant. The congregated bundles appear, and the porosity increases with longer etching time. Especially for the 3-h-etched sample, the inserted image of the congregated tips shows that the tips of the nanowires were etched in excess and the tips are fragmentary. The TEM image shows that the wire consists of the net-like silicon framework. This is also different from the earlier publication [31], in which the authors figured out the H_2O_2 concentration is the key factor of the porosity varieties, while the etching time could only increase the thickness of the porous layer. This could be well explained by the formation mechanism of the nanopores listed below.

The length variation of the nanowires with H_2O_2 concentration and etching time is shown in Fig. 3. The chemical etching of Si includes the reactions listed below.

$$2Ag + H_2O_2 + 2H^+ \rightarrow 2Ag^+ + 2H_2O \quad (1)$$

$$Si + 4Ag^+ + 6F^- \rightarrow 4Ag + SiF_6^{2-} \quad (2)$$

The total reaction

$$Si^0 + 2H_2O_2 + 6F^- + 4H^+ \rightarrow [SiF_6]^{2-} + 4H_2O \quad (3)$$

From Eq. 3, the potential for the etching process could be expressed as below.

$$\Delta E = \Delta E^0 - \frac{0.059}{4}\log\frac{[SiF_6^{2-}]}{[H_2O_2]^2[H^+]^4[F^-]^6} \quad (4)$$

The increase in H_2O_2 concentration could enhance the potential for the etching process, which indicates that the etching reaction is more thermodynamically favored and the etching could be accelerated. Therefore, the length of the nanowires is not only time dependent, but also relies on the oxidant concentration. Figure 3b shows that the length of SiNWs etched for 3 h is a bit lower than expected. This could be attributed to the serious conglomeration of the SiNWs.

The etching process of the porous SiNWs could be elucidated in Fig. 4. As the catalyst, the AgNPs are

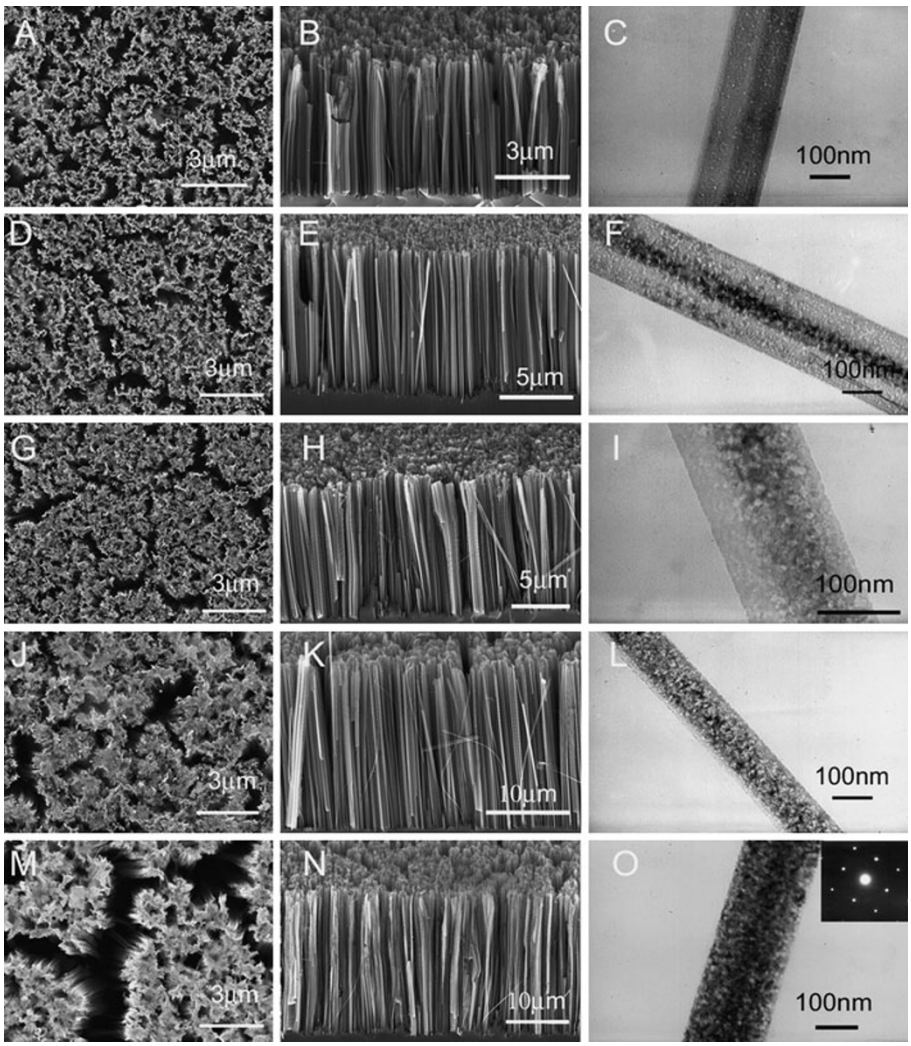

Fig. 1 SEM and TEM images of the variable morphology of porous SiNWs etched with different H_2O_2 concentrations. **a–c** 0.1 M H_2O_2, **d–f** 0.2 M H_2O_2, **g–i** 0.3 M H_2O_2, **j–l** 0.4 M H_2O_2, **m–o** 0.5 M H_2O_2. The SAD pattern is shown in the *inset* (**o**)

oxidized into Ag^+ ions by H_2O_2. The Ag^+ ions extract electrons from Si nearby and are deoxidized into Ag again. The Si atoms around are oxidized and dissolved, leading to the etching of the silicon surface and the formation of the vertical SiNW arrays [32]. However, during the etching process, the Ag^+ ions could not be recovered to Ag totally. Ag^+ ions with certain concentration around the AgNPs would diffuse out to the tips of the SiNWs, where the concentration of Ag^+ ions is lower. For the lightly doped silicon wafer, the Ag^+ ions along with the SiNWs are difficult to be deoxidized into smaller AgNPs as the lack of defective sites for new nucleation. So the diffused Ag^+ cannot etch the sidewalls of the SiNWs and no porous structure appears. However, for the heavily doped silicon wafers, the dopants could induce amount of weak defective points in the silicon lattices. These defective points could serve as the nucleation centers. When the Ag^+ ions near the defective points reach a critical concentration, the Ag^+ will nucleate on the side walls or the tips of the SiNWs and the smaller AgNPs appear. These newly formed AgNPs open new etching pathways on the SiNWs and facilitate the formation of the nanopores. Furthermore, the nucleation of the AgNPs on the side walls would also reduce the Ag^+ concentration and accelerates the Ag^+ diffusion. When the Ag^+ ions concentration reaches the critical value again, new nucleation occurs. This could be confirmed by our results listed in Fig. 2, the porosity of the nanowires increases with the etching time, which indicates that new AgNPs appear and new nanopores form with time. It could also be found that some nanopores overlap on the side walls, especially for the SiNWs etched with longer time. It is because new AgNPs nucleation takes place near the defects distributed on the wires, some nucleation centers stay near the formed nanopores, and the newly etched pores would overlap with the original ones. It could also explain why the nanopores seem to grow larger with times. From this mechanism, we could deduce that the side walls on the topside of the wires have higher porosity compared with the downside. It is confirmed by the TEM images in Fig. 5. As the nanowires were scraped from the wafers, the cuts of

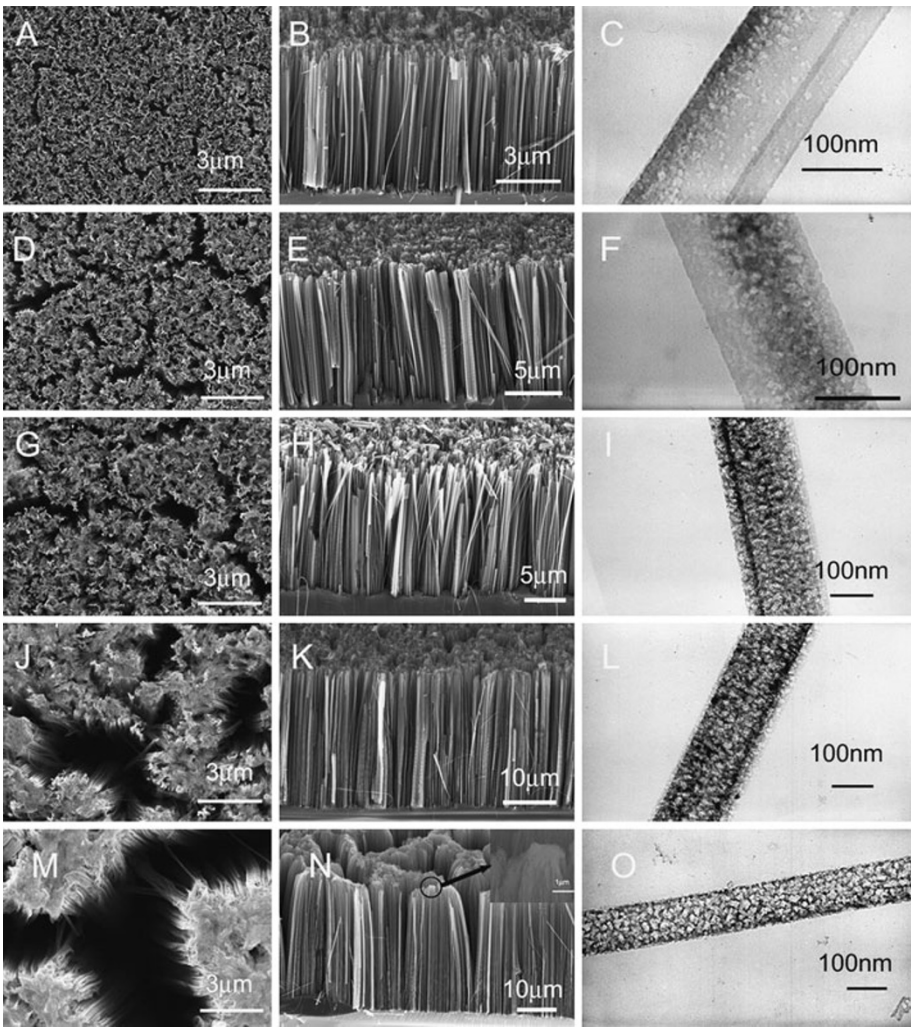

Fig. 2 SEM and TEM images of the variable morphology of porous SiNWs etched with 0.3 M H_2O_2 for different times. **a–c** 30 min, **d–f** 60 min, **g–i** 90 min, **j–l** 120 min, **m–o** 180 min. The *inset* in **n** is the higher magnification image as marked

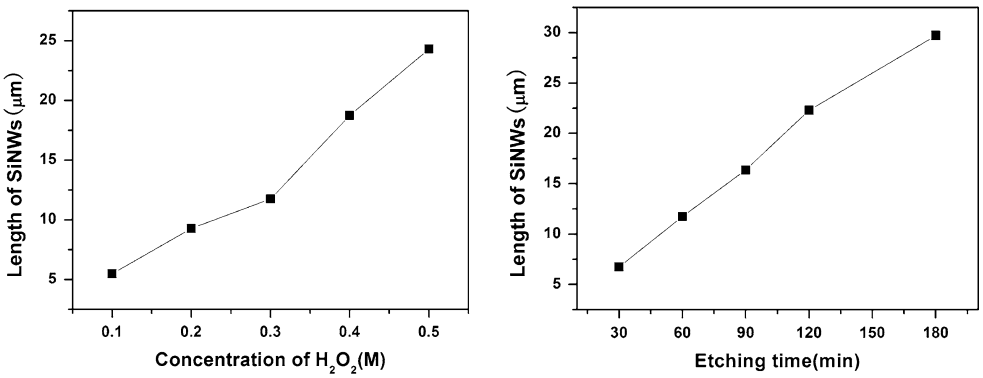

Fig. 3 The lengths of the porous SiNWs depend on **a** H_2O_2 concentrations and **b** etching times

the wires are trim. However, the tips are fragmentary as shown in the SEM image. Figure 5b–d correspond to the different sections on the same nanowire marked in Fig. 5a. It could be clearly seen that the porosity increases and the nanopores grow larger from the bottom to the top tip. The increase in H_2O_2 concentrations could accelerate the oxidation of Ag and increase the Ag^+ ions concentrations, leading to more additional etching pathways and higher porosity. It could be concluded that the doping lever of the silicon wafer, the H_2O_2 concentration and the etching time are the key factors for the nanopores formation on the SiNWs.

The room temperature PL measurement was carried out to study the optical properties of the porous SiNWs. Figure 6a and b display the PL spectrums of the porous SiNWs with different H_2O_2 concentrations and etching

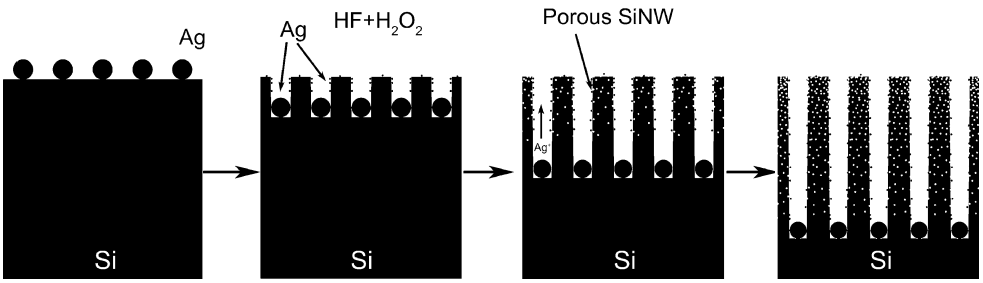

Fig. 4 Schematic view of the formation mechanism of porous SiNW arrays

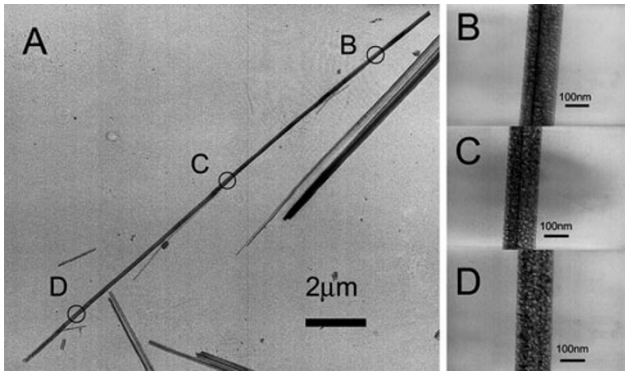

Fig. 5 TEM image of different sections on the same wire. **a** low magnification image of the SiNW, **b–d** corresponding higher magnification images marked in **a**

times. As the increase in the H_2O_2 concentrations or etching times, the porosity of the nanowires increases and leads to the PL intensity enhancement. The PL intensity of SiNWs etched with 0.5 M H_2O_2 is almost 35 times as high as the samples etched with 0.1 M H_2O_2. When the sample was etched for 3 h, an increase in the PL intensity by a factor of 40 is observed, compared with the 30 min-etched sample. However, it is unexpected to find that PL peaks of the samples with higher porosity seem to "red-shift" and are not well symmetrical. It is thought that higher porosity would decrease the size of the silicon nanostructure, which could lead to the blue-shift of the PL peak due to the quantum confinement effect. In order to explain this phenomenon, we decomposed the PL spectrums shown in Fig. 7a. It is displayed that the PL spectrum is composed of two elementary PL bands with the peaks around 750 and 850 nm, respectively. This indicates that the PL spectrums shown in Fig. 6a and b have two origins. We also measure the PL spectrums of the samples treated with HNO_3 but without HF solution, which are considered to have an oxide layer on the surfaces. It is found that the PL peaks are fixed at $\sim$730 nm for all the samples. The PL intensity varieties with the preparation parameters are similar with the samples with HF treatment. These PL peaks at 730 nm are close to the 750-nm PL peaks decomposed from the HF-treated samples. The deviation should be attributed to the decomposition of the observed PL spectrum with two ideal Gauss peaks. It is supposed that the HF-treated samples are partially oxidized when exposing in the air and the PL spectrums in Fig. 6a and b compose of two PL bands. The peak fixed at 750 nm arises from the silicon nanostructure coated with a thin oxide layer, while the one at 850 nm should be the emission of the localized excitation in the nanoporous structure.

The FTIR analysis was carried out to confirm our supposition. As is shown in Fig. 8, the characteristic asymmetric stretching signals of Si–O–Si Bridge distribute between 1,000 and 1,300 cm^{-1} in the spectrum. The signals include a strong band at $\sim$1,080 cm^{-1} (adjacent oxygen atoms execute the asymmetric stretching motion in phase with each other) and a shoulder at $\sim$1,200 cm^{-1} (adjacent oxygen atoms execute the asymmetric stretching motion 180° out of phase). The peaks between 2,050 and 2,170 cm^{-1} represent the absorption due to different vibration modes of Si–H_x bonds, while the peak at 2,248 cm^{-1} corresponds to the Si–H stretching mode in O_3-SiH. It is shown that the signal from Si–O bond is much stronger for the HNO_3-treated samples. The small peaks around 2,100 and 2,248 cm^{-1} indicate that there are still small amount of surface hydrogen bonds. After HF treatment, the signal of Si–O bond still exists but falls down. As the previous oxide layer was dissolved in the HF solution, these weak peaks should be due to the natural oxidation in the air. The stronger Si–H signal reflects the fact that the surface is mainly terminated by Si–H_x bonds. These FTIR results approve our deduction above.

Furthermore, we study the elementary PL intensity of the HF treated samples with different processing parameters. As is shown in Fig. 7, for the samples with lower porosity, the peak at 750 nm is stronger than the one at 850 nm. When the porosity increases, both the PL intensities increase. However, the emission intensity from the local nanoporous structure enhances more quickly and takes up the leading place. This is more obvious in Fig. 7c, the intensity of the 850-nm PL peak is twice as high as the peak at 750 nm for the 3-h-etched sample. This explains why the PL peaks of the HF-treated samples seem to "red-shift" with longer etching times or higher H_2O_2 concentrations.

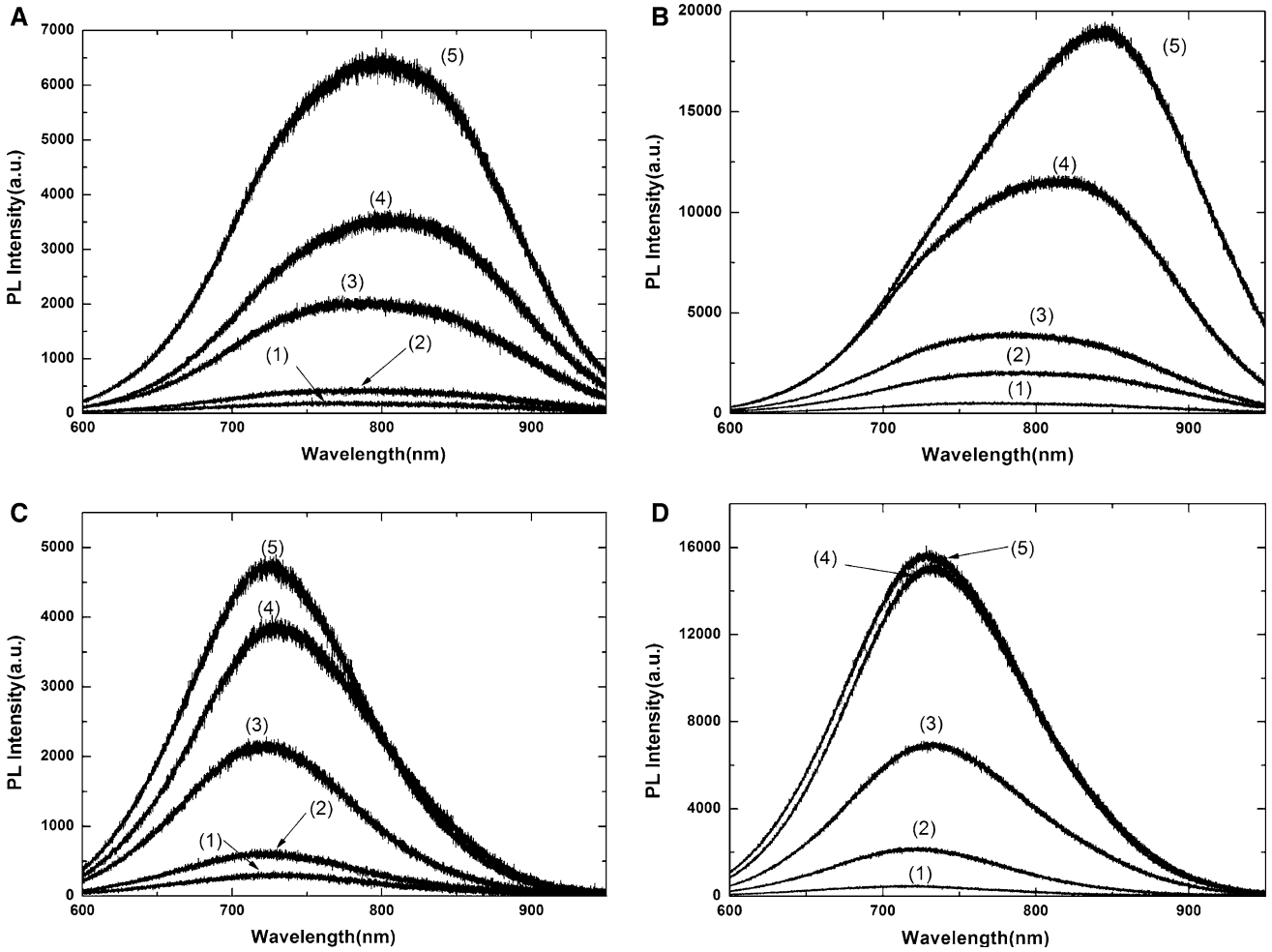

Fig. 6 The PL spectrums of the SiNWs with different preparation parameters. **a**,**b** Correspond to the samples with HF treatment, **c**,**d** correspond to the samples with HNO_3 treatment. (*1*)–(*5*) in **a** and **c** correspond to the SiNWs etched for 60 min with the H_2O_2 concentrations of 0.1, 0.2, 0.3, 0.4 and 0.5 M, respectively. (*1*)–(*5*) in b and **d** correspond to the SiNWs etched with 0.3 M H_2O_2 for 30, 60, 90, 120, and 180 min, respectively

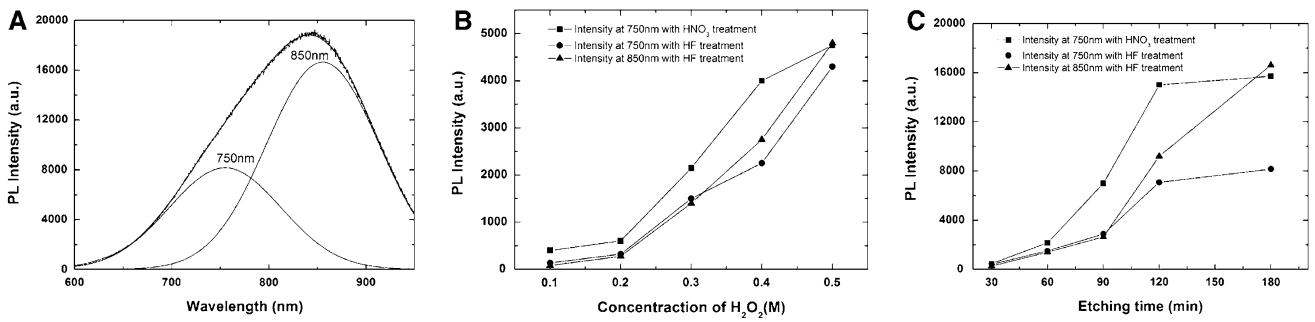

Fig. 7 **a** The decomposition of the PL spectrum of the SiNWs treated with HF and the PL intensity varieties of the elementary bands with **b** H_2O_2 concentrations and **c** etching times

Conclusions

In summary, we carried out electroless etching on the highly doped *n*-type silicon (100) wafers to synthesize the porous SiNW arrays. We found that longer etching time or higher H_2O_2 concentration could facilitate the diffusion and nucleation of Ag^+ ions and effectively enhance the porosity of the nanowires. The PL intensity could be

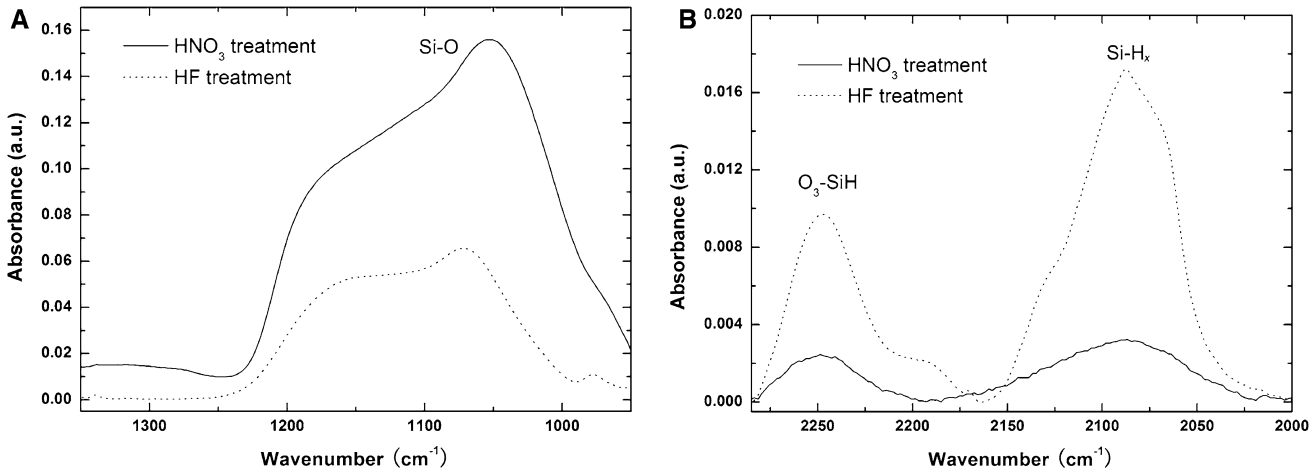

Fig. 8 FTIR spectra of the SiNWs treated with HNO_3 and HF

effectively enhanced by the increased porosity. Further studies including the decomposition of the PL spectrum and the FTIR analysis confirm that the surface of the HF-treated porous SiNWs are composed of Si–H_x and Si–O bonds, corresponding to the peaks at 850 and 750 nm, respectively. The emission intensity from the local porous structure quickly enhances with the porosity and takes up the leading place of the PL spectrum, resulting in the "red-shift" observed. These porous SiNWs combine the physical properties of SiNWs and PS and could lead to opportunities for new generation of nanoscale optoelectronic devices.

Acknowledgments This work was supported by Tsinghua National Laboratory for Information Science and Technology (TNList) Cross-discipline Foundation.

References

1. Y. Huang, X.F. Duan, Y. Cui, L.J. Lauhon, K.H. Kim, C.M. Lieber, Science **294**, 1313 (2001)
2. Y. Ahn, J. Dunning, J. Park, Nano Lett. **5**, 1367 (2005)
3. Q.L. Li, S.M. Koo, M.D. Edelstein, J.S. Suehle, C.A. Richter, Nanotechnology **18**, 315202 (2007)
4. S.M. Koo, Q.L. Li, M.D. Edelstein, C.A. Richter, E.M. Vogel, Nano Lett. **5**, 2519 (2005)
5. Z. Li, Y. Chen, X. Li, T.I. Kamins, K. Nauka, R.S. Williams, Nano Lett. **4**, 245 (2004)
6. K. Yang, H. Wang, K. Zou, X.H. Zhang, Nanotechnology **17**, S276 (2006)
7. G.F. Zheng, F. Patolsky, Y. Cui, W.U. Wang, C.M. Lieber, Nat. Biotechnol. **23**, 1294 (2005)
8. Y. Cui, Q.Q. Wei, H.K. Park, C.M. Lieber, Science **293**, 1289 (2001)
9. K.Q. Peng, X. Wang, S.T. Lee, Appl. Phys. Lett. **95**, 243112 (2009)
10. C.K. Chan, H.L. Peng, G. Liu, K. McIlwrath, X.F. Zhang, R.A. Huggins, Y. Cui, Nat. Nanotechnol. **3**, 31 (2008)
11. K.Q. Peng, J.S. Jie, W.J. Zhang, S.T. Lee, Appl. Phys. Lett. **93**, 033105 (2008)
12. B.Z. Tian, X.L. Zheng, T.J. Kempa, Y. Fang, N.F. Yu, G.H. Yu, J.L. Huang, C.M. Lieber, Nature **449**, 885 (2007)
13. E.C. Garnett, P.D. Yang, J. Am. Chem. Soc. **130**, 9224 (2008)
14. K.Q. Peng, X. Wang, S.T. Lee, Appl. Phys. Lett. **92**, 163103 (2008)
15. N.A. Hill, K.B. Whaley, Phys. Rev. Lett. **75**, 1130 (1995)
16. P. Mutti, G. Ghislotti, S. Bertoni, L. Bonoldi, G.F. Cerofolini, L. Meda, E. Grilli, M. Guzzi, Appl. Phys. Lett. **66**, 851 (1995)
17. L.T. Canham, Appl. Phys. Lett. **57**, 1046 (1990)
18. L.T. Canham, W.Y. Leong, M.I.J. Beale, T.I. Cox, L. Taylor, Appl. Phys. Lett. **61**, 2563 (1992)
19. X. Li, P.W. Bohn, Appl. Phys. Lett. **77**, 2572 (2000)
20. K.Q. Peng, Y.J. Yan, S.P. Gao, J. Zhu, Adv. Mater. **14**, 1164 (2002)
21. M.L. Zhang, K.Q. Peng, X. Fan, J.S. Jie, R.Q. Zhang, S.T. Lee, N.B. Wong, J. Phys. Chem. C **112**, 4444 (2008)
22. K.Q. Peng, Y.J. Yan, S.P. Gao, J. Zhu, Adv. Funct. Mater. **13**, 127 (2003)
23. K.Q. Peng, Z.P. Huang, J. Zhu, Adv. Mater. **16**, 73 (2004)
24. K.Q. Peng, Y. Xu, Y. Wu, Y.J. Yan, S.T. Lee, J. Zhu, Small **1**, 1062 (2005)
25. J. Huo, R. Solanki, J.L. Freeouf, J.R. Carruthers, Nanotechnology **15**, 1848 (2004)
26. S. Kim, C.O. Kim, D.H. Shin, S.H. Hong, M.C. Kim, J. Kim, S.H. Choi, T. Kim, R.G. Elliman, Y.M. Kim, Nanotechnology **21**, 205601 (2010)
27. T.K. Sham, S.J. Naftel, P.S.G. Kim, R. Sammynaiken, Y.H. Tang, I. Coulthard, A. Moewes, J.W. Freeland, Y.F. Hu, S.T. Lee, Phys. Rev. B **70**, 045313 (2004)
28. M.W. Shao, L. Cheng, M.L. Zhang, D.D.D. Ma, J.A. Zapien, S.T. Lee, X.H. Zhang, Appl. Phys. Lett. **95**, 143110 (2009)
29. M.H. Kim, I.S. Kim, Y.H. Park, T.E. Park, J.H. Shin, H.J. Choi, Nanoscale Res. Lett. **5**, 286 (2010)
30. A.I. Hochbaum, D. Gargas, Y.J. Hwang, P.D. Yang, Nano Lett. **9**, 3550 (2009)
31. Y.Q. Qu, L. Liao, Y.J. Li, H. Zhang, Y. Huang, X.F. Duan, Nano Lett. **9**, 4539 (2009)
32. K.Q. Peng, A.J. Lu, R.Q. Zhang, S.T. Lee, Adv. Funct. Mater. **18**, 3026 (2008)